Probability maximization of magnetization switching by spin-orbit torques generated by a ferromagnet

Tomohiro Taniguchi [1,*] Shinji Isogami [2] Shuji Okame,[3] Katsuyuki Nakada,[3]
Tomoyuki Sasaki,[3] Seiji Mitani,[2] and Masamitsu Hayashi[2,4]

[1]*National Institute of Advanced Industrial Science and Technology (AIST), Research Center for Emerging Computing Technologies, Tsukuba, Ibaraki 305-8568, Japan*

[2]*National Institute for Materials Science, Tsukuba 305-0047, Japan*

[3]*Advanced Products Development Center, Technology & Intellectual Property HQ, TDK Corporation, Ichikawa, Chiba 272-8558, Japan*

[4]*Department of Physics, The University of Tokyo, Tokyo 113-8654, Japan*

(Received 27 January 2025; revised 22 February 2025; accepted 28 February 2025; published 17 March 2025)

Spin-orbit torques (SOTs) caused by spin currents generated in a ferromagnetic electrode enable a fast and deterministic magnetization switching. One SOT (y-SOT), polarized orthogonal to both electric current flowing in the electrode and easy axis of a ferromagnetic free layer, causes fast magnetization instability. The other SOT (z-SOT) points to the easy-axis direction and leads to the deterministic switching. Here, we evaluate the magnetization switching probability by these SOTs for various values of electric current density and the ratio of two SOTs from numerical simulation of the Landau-Lifshitz-Gilbert (LLG) equation. It is found that the switching probability is maximized when the electric current density is close to a critical value for the magnetization destabilization solely by the y-SOT. The origin of such a current dependence is investigated by analyzing temporal dynamics, spectra of the magnetization distribution, and a steady-state solution of the LLG equation. We reveal that the maximization of the switching probability originates due to two different switching behaviors. In the low current region, the magnetization in some trials remains near the initial state because of the weak y-SOT, and thus, the switching error occurs. The number of such trials, which represents the switching error, decreases as the electric current density increases because both y and z-SOTs prompt the switching. In the large current region, the large y-SOT immediately tilts the magnetization toward the switched direction. However, since the y-SOT prefers an in-plane magnetized state, the switching error due to a probabilistic return to the initial state after turning off the electric current density occurs. The switching error in this region tends to increase with increasing current density. As a result, the switching probability is optimized when the electric current density is close to the critical value.

DOI: 10.1103/PhysRevB.111.094420

I. INTRODUCTION

Spin-orbit torque (SOT) driven magnetization dynamics [1–3] has attracted significant attention to manipulate the magnetization in nanostructured ferromagnets. SOT originates from pure spin current generated by spin-orbit coupling in nonmagnetic electrode [4–6]. The spin polarization of SOT points to a direction orthogonal to both electric and spin currents. (In this paper, we use a Cartesian coordinate where the electric and spin currents flow along x- and z-directions, respectively, and therefore, the SOT points to the y direction). One of the advantages of SOT, compared to spin-transfer torque (STT) [7,8] in the conventional two-terminal structures [9–15], is the fast magnetization destabilization in a perpendicularly magnetized ferromagnet. SOT directly moves the magnetization from the stable (z) direction to an in-plane ($\parallel y$) direction without accompanying magnetization precession. This is in contrast to the conventional STT switching [16] that costs a much longer time. However, SOT fixes the magnetization to the y direction, and therefore, the magnetization switching becomes probabilistic [17]. Although the switching becomes deterministic by applying an external magnetic field along the x direction, this method is not preferable from a practical viewpoint. Therefore, various approaches for magnetic field-free switching have been proposed, such as utilizing lateral structure asymmetry [18], tilted magnetic anisotropy [19,20], exchange bias from the antiferromagnet [21], interlayer exchange coupling [22], and STT assistance [23–27].

Another solution for magnetic field-free switching is to use SOTs caused by spin currents generated in ferromagnetic electrode, which have been studied both theoretically [28–37] and experimentally [38–45]. An advantage utilizing such SOTs is the ability to manipulate the torque direction. For example, the SOT due to the spin anomalous Hall effect [28,38,41,43] is parallel to the magnetization direction in the ferromagnetic electrode. SOTs due to the spin-orbit filtering and spin-orbit precession effects near the ferromagnetic/nonmagnetic interface [29,30,39,42] and bulk spin Hall effect in the ferromagnet [44] generate two kinds of SOTs pointing to the y and $\mathbf{e}_y \times \mathbf{p}$ directions, where $\mathbf{e}_k$ $(k = x, y, z)$ and $\mathbf{p}$ are the unit vectors in the k direction and in the magnetization direction of the ferromagnetic electrode. Therefore, we

*Contact author: tomohiro-taniguchi@aist.go.jp

can excite both SOTs directed along y and z, called y and z-SOTs for simplicity in this paper, acting on the top free layer simultaneously when a ferromagnetic electrode is magnetized along the x direction ($\mathbf{p} = \mathbf{e}_x$). The y-SOT induces a fast magnetization instability from the easy axis while the z-SOT results in a deterministic switching. Accordingly, SOTs generated from a ferromagnetic electrode are expected to be useful for realizing fast and deterministic magnetization manipulation.

In this work, we evaluate the magnetization switching probability by solving the Landau-Lifshitz-Gilbert (LLG) equation with both y and z-SOTs at finite temperature. It is found that the switching probability is maximized when the current density is close to a critical value for the magnetization destabilization solely by the y-SOT, and further increase of the electric current density leads to a reduction of the switching probability (or equivalently, the error rate increases). This is contrary to the intuition that the switching probability increases as the electric current density increases, as found in the previous works for both STT and SOT switchings [15,17]. The origin of such a current dependence of the switching probability is investigated from temporal dynamics, spectra of the magnetization distribution, and an analytical solution of the LLG equation in a steady state. These analyses reveal that the maximization of the switching probability is a result of the competition between two switching behaviors. In the low current region, the z-SOT is necessary for the switching while the y-SOT contributes to reducing the time necessary to escape from the initial state. When the current magnitude is small, the magnetization remains near the initial state for some trials and causes the switching error. Thus, the switching probability increases as the electric current density increases. When the electric current density exceeds the critical value, on the other hand, the magnetization immediately changes its direction and reaches a steady state. The magnetization direction in the steady state is determined by the balance between the two SOTs: it changes from the switched state to a state along the film plane as the electric current density is increased. This change of the steady state causes a probabilistic return of the magnetization to the initial state due to thermal fluctuation after turning off the current and becomes an origin of an error. The switching probability is therefore optimized when the electric current density is close to the critical value. The result indicates that application of a large electric current density does not guarantee a reduction of the switching error and implies a condition for maximizing the switching probability.

This paper is organized as follows. In Sec. II, we describe the system under study and show the switching probability evaluated by numerical simulation of the LLG equation. In Sec. III, the origin of the switching error is studied by analyzing the temporal dynamics, evaluating the magnetization distribution, and solving the LLG equation analytically. Section IV is devoted to the conclusion.

II. NUMERICAL SIMULATION

In this section, we first introduce the system under study and then discuss the dependence of the switching probability on various system parameters.

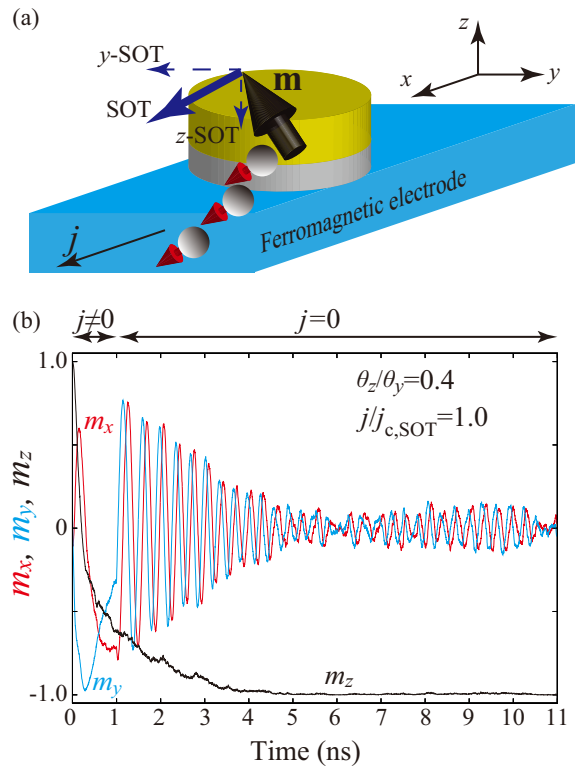

FIG. 1. (a) Schematic illustration of SOT devices. Electric current density j flowing in a bottom ferromagnetic electrode generates spin current, whose spin polarization can be decomposed into y and z components. Thus, SOT acting on magnetization $\mathbf{m}$ in a ferromagnetic free layer can also be decomposed into the y and z-SOTs. (b) An example of temporal magnetization dynamics for $\vartheta_z/\vartheta_y = 0.4$ and $j/j_{c,\mathrm{SOT}} = 1.0$. The electric current density is finite from $t = 0$ to $t = 1.0$ ns while it is turned off at $t = 1.0$ ns. The magnetization is regarded to be switched when m_z after 10 ns from turning off j satisfies $m_z < 0$.

A. Landau-Lifshitz-Gilbert equation

Figure 1(a) shows a schematic illustration of the system. The top ferromagnetic free layer and the bottom ferromagnetic electrode are separated by a thin nonmagnetic spacer. By applying electric current density j flowing in the x direction to the bottom ferromagnetic electrode, spin currents polarized in the y and z directions are generated at the interface [29,30,39,42] and bulk [44]. These spin currents are injected into the top ferromagnetic free layer and exert y and z-SOTs. The magnetization dynamics excited in a perpendicularly magnetized free layer by such SOTs is described by the LLG equation,

$$\frac{d\mathbf{m}}{dt} = -\gamma\mathbf{m}\times\mathbf{H} - \gamma H_{\mathrm{SOT},y}\mathbf{m}\times(\mathbf{e}_y\times\mathbf{m}) - \gamma H_{\mathrm{SOT},z}\mathbf{m}\times(\mathbf{e}_z\times\mathbf{m}) + \alpha\mathbf{m}\times\frac{d\mathbf{m}}{dt}, \quad (1)$$

where $\mathbf{m}$ is the unit vector pointing in the magnetization direction in the free layer. The magnetic field $\mathbf{H} = H_{\mathrm{K}}m_z\mathbf{e}_z$ corresponds to the perpendicular magnetic anisotropy field ($H_{\mathrm{K}} > 0$): other magnetic fields, e.g., the external magnetic field, are neglected in this study. The parameters γ and α

TABLE I. Parameters used in the numerical calculations: M, saturation magnetization; H_K, perpendicular magnetic anisotropy field; γ, gyromagnetic ratio; α, Gilbert damping constant; d, thickness of the free layer; V, volume of the free layer; ϑ_y, spin Hall angle of the y-SOT.

Quantity	Value
M	1500 emu/cm^3
H_K	1.172 kOe
γ	1.764×10^7 rad/(Oe s)
α	0.030
d	1 nm
V	$d\times\pi\times30^2$ nm^3
ϑ_y	0.30

are the gyromagnetic ratio and the Gilbert damping constant, respectively. The second and third terms on the right-hand side of Eq. (1) describe the y and z-SOTs. The k component ($k = y, z$) of the SOT strength is

$$H_{\mathrm{SOT},k} = \frac{\hbar\vartheta_k j}{2eMd}, \tag{2}$$

where the parameters M and d are the saturation magnetization and the thickness of the free layer. The k component of the spin Hall angle is denoted as ϑ_k. The past experiments indicate that $|\vartheta_z/\vartheta_y| < 1$ [42,44]. In addition, if the z-SOT is much stronger than the y-SOT, the switching becomes similar to the conventional STT switching, which has been studied previously. Therefore, we consider the parameter region of $|\vartheta_z/\vartheta_y| \leqslant 1$ in this work. A recent experiment showed that ϑ_z/ϑ_y in Co-Ni ferromagnets changes as the material concentrations change [44]. Therefore, the material investigation showing a large ϑ_z, which originates from the spin-orbit precession effect at the interface [29,30] and spin Hall precession effect inside the bulk [44], will be one research direction for achieving high switching probability. The values of the parameters are summarized in Table I [46]. Here H_K is set such that the thermal stability $\Delta_0 = MH_KV/(2k_BT)$, with the volume V and temperature T at room temperature ($T = 300$ K), is equal to 60.

For later discussion, it is convenient to introduce critical current densities. The definition of the critical current density is that, when the current density becomes larger than the critical value, the magnetization in the presence of torque is no longer stable near the initial state at zero temperature. In the presence of the y-SOT only, the critical current density is given by [47]

$$j_{\mathrm{c,SOT}} = \frac{eMd}{\hbar\vartheta_y}H_K. \tag{3}$$

Using the values in Table I, the critical current density by the y-SOT, given by Eq. (3), is 89 MA/cm^2. We note that the formula similar to Eq. (3) was derived in Ref. [48] for a different purpose. Recall also that Ref. [47] assumes that the trajectory of the magnetization switching satisfies $m_y = 0$ to derive Eq. (3). This assumption is valid when the current pulse has a finite rise time, while it is not applicable to, for example, a step-function-like input [49]; however, Eq. (3) works well to estimate the instability by the y-SOT in many cases. In the presence of the z-SOT only, the critical current density is the same with that for two-terminal MRAM driven by spin-transfer torque [16,50]

$$j_{\mathrm{c,STT}} = \frac{2e\alpha Md}{\hbar\vartheta_z}H_K. \tag{4}$$

Usually, the value of $j_{\mathrm{c,SOT}}$ given by Eq. (3) is much larger than $j_{\mathrm{c,STT}}$ given by Eq. (4) due to the small quantity $\alpha(\ll 1)$, which only appears in Eq. (4) [51]. This is because the y-SOT induced magnetization destabilization is a result of the competition between the y-SOT and the precessional torque [49], while the conventional STT switching is a result of the competition between STT and the damping torque [16]. Strictly speaking, the condition $j_{\mathrm{c,SOT}} > j_{\mathrm{c,STT}}$ is satisfied when $\vartheta_z/\vartheta_y > 2\alpha$ holds. In the following calculations, we change the value of ϑ_z/ϑ_y from 0 to 1 with an increment 0.05. Therefore, $j_{\mathrm{c,SOT}} > j_{\mathrm{c,STT}}$ is satisfied in general, except for a narrow parameter region $\vartheta_z/\vartheta_y \sim 0$ to 0.1. In the following, we use $\vartheta_z/\vartheta_y = 0.4$ as a representative case. Under such parameter set, $j_{\mathrm{c,STT}} = 13$ MA/cm^2. We therefore have $j > j_{\mathrm{c,STT}}$ when $j > j_{\mathrm{c,SOT}}$.

B. Definition of switching probability

We add a random torque $-\gamma\mathbf{m}\times\mathbf{h}$ to the right-hand side of Eq. (1) to describe the thermally activated magnetization dynamics. Component h_k ($k = x, y, z$) of the random field $\mathbf{h}$ satisfies the fluctuation-dissipation theorem [52],

$$\langle h_k(t)h_\ell(t')\rangle = \frac{2\alpha k_BT}{\gamma MV}\delta(t-t'), \tag{5}$$

where T and V are the temperature and the volume of the free layer. A numerical method to solve Eq. (1) using Eq. (5) was described in our previous work [46,53].

In the present study, we solve the LLG equation with different random torque 10^7 times. In each trial, we initially solve the LLG equation without SOTs for 10 ns with the initial condition of $\mathbf{m} = +\mathbf{e}_z$ to obtain distributed initial states induced by thermal fluctuation. Then we solve the LLG equation with a finite current density j, where its pulse width is 1 ns. After that, we solve the LLG equation without SOTs for a duration of 10 ns. The trial is regarded as to be magnetization switching when $m_z < 0$ at this moment. Figure 1(b) shows an example of the magnetization dynamics in the presence of thermal fluctuation, where $j/j_{\mathrm{c,SOT}} = 1.0$ and $\vartheta_z/\vartheta_y = 0.4$. According to the definition, this case is classified as magnetization switching. By repeating such trials 10^7 times, the switching probability is obtained.

C. Switching probability

Figures 2(a)–2(d) show the dependence of the switching probability on ϑ_z/ϑ_y for $j/j_{\mathrm{c,SOT}} = 0.8$, 1.0, 1.5, and 2.0, respectively. In all cases, the switching probability increases monotonically with ϑ_z/ϑ_y increases. This is reasonable because the z-SOT moves the magnetization to the switched direction. We, however, notice that the details of the switching probability are different.

For small ϑ_z/ϑ_y, the switching probability is smaller than 0.5 when the current is small [$j/j_{\mathrm{c,SOT}} < 1.0$, Fig. 2(a)]

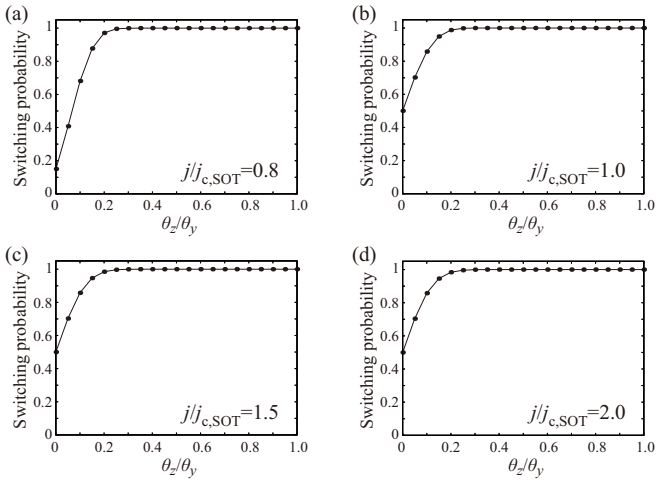

FIG. 2. Dependence of the magnetization switching probability on ϑ_z/ϑ_y for the electric current densities with respect to the critical value, $j/j_{c,SOT}$, of (a) 0.8, (b) 1.0, (c) 1.5, and (d) 2.0.

while it is approximately 0.5 or larger for the other cases [$j/j_{c,SOT} \geqslant 1.0$, Figs. 2(b)–2(d)]. Recall that the y-SOT induces a fast destabilization of the magnetization and moves it to the in-plane direction (parallel to the y axis) when the electric current density exceeds $j_{c,SOT}$. It is therefore reasonable that the switching probability is 0.5 for $j/j_{c,SOT} \geqslant 1.0$ and $\vartheta_z = 0$. When the electric current density is smaller than $j_{c,SOT}$, however, the destabilization of the magnetization by the y-SOT becomes weaker, and thus, the magnetization does not reach the in-plane direction in many cases. As a result, the switching probability becomes much smaller than 0.5 for a small ϑ_z/ϑ_y when $j/j_{c,SOT} < 1$, as shown in Fig. 2(a).

For $j/j_{c,SOT} \geqslant 1.0$ [Figs. 2(b)–2(d)], one may consider the switching probability is approximately independent of the electric current density. However, the details show a nontrivial behavior. In Fig. 3, we show an enlarged view of the switching probabilities of Fig. 2 for $0.2 \leqslant \vartheta_z/\vartheta_y \leqslant 0.4$. We also rearrange the probabilities as a function of the electric current density with respect to $j_{c,SOT}$ in Fig. 4, while

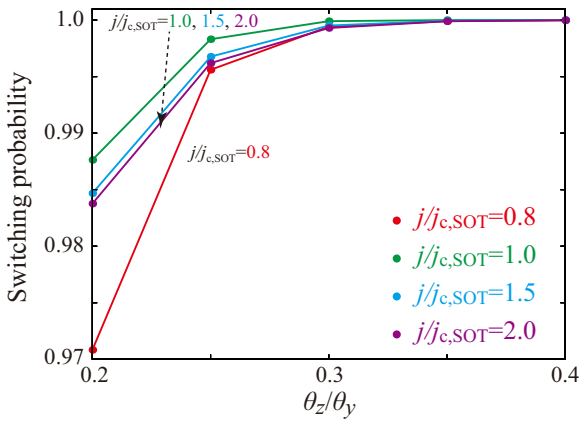

FIG. 3. An enlarged view of the magnetization switching probability in Fig. 2 near $0.2 \leqslant \vartheta_z/\vartheta_y \leqslant 0.4$, where the electric current density with respect to the critical value, $j/j_{c,SOT}$, of (a) 0.8 (red), (b) 1.0 (green), (c) 1.5 (blue), and (d) 2.0 (purple).

TABLE II. Switching probabilities for various $j/j_{c,SOT}$ and ϑ_z/ϑ_y obtained from 10^7 trials of the LLG equation.

$\frac{j}{j_{c,SOT}}$	$\frac{\vartheta_z}{\vartheta_y} = 0.20$	0.25	0.30	0.35	0.40
0.8	0.9708238	0.9956011	0.9994168	0.9999065	0.9999861
1.0	0.9876308	0.9983098	0.9999070	0.9999991	1.0000000
1.5	0.9846845	0.9967647	0.9995187	0.9999465	0.9999968
2.0	0.9837671	0.9961923	0.9993042	0.9998977	0.9999879

their numerical values are listed in Table II. It shows that the switching probability is maximized near $j/j_{c,SOT} = 1.0$. One might consider that the difference of the switching probability for the different electric current density is negligible in these cases. However, their differences are non-negligible for practical purposes such as magnetoresistive random access memory applications. For example, an error rate less than 10^{-3} for storage memory or 10^{-9} for working memory is required [15,54,55]. In such applications, it will be required to clarify the origin of the current dependence of the switching probability. Note that the switching probability for a large current region ($j/j_{c,SOT} \gtrsim 1.0$) decreases as the electric current density increases. The result is against the intuition that the switching probability increases as the electric current density increases, which has been found in both STT and SOT switchings [17,53]. Therefore, we develop theoretical analyses to clarify the current dependence of the switching probability in the present system.

III. THEORETICAL ANALYSIS

In this section, we investigate the origin of the switching error found in Sec. II. We analyze the temporal dynamics in details, evaluate the spectra of the magnetization distribution, and derive an analytical solution of the LLG equation in a steady state.

A. Temporal dynamics

We firstly study the temporal dynamics from the numerical solution of the LLG equation. Figure 5 shows examples of the time development of m_z in the presence of the electric current density ($0 \leqslant t \leqslant 1.0$ ns), where the electric current density is $j/j_{c,SOT} = 0.8$ (red), 1.0 (green), 1.5 (blue), and 2.0 (purple) while $\vartheta_z/\vartheta_y = 0.4$. First, the time scale of the temporal change of m_z becomes shorter as the electric current density increases. This is because strong SOTs drive fast magnetization dynamics. In particular, m_z reaches a steady state for relatively large electric current densities ($j/j_{c,SOT} = 1.5$ and 2.0) while it seems to be on a way to a steady state for relatively small electric current densities ($j/j_{c,SOT} = 0.8$ and 1.0); see also Appendix. Second, when the electric current density is turned off ($t = 1.0$ ns), m_z becomes closer to the switched state ($m_z = -1$) when the electric current density is small, or in other words, the magnetization stays close to the in-plane direction when the electric current is large. This is because a large electric current density leads to a strong y-SOT, which prefers to fix the magnetization to the y direction. In Sec. III C, we verify this finding from an analytical solution of the LLG equation.

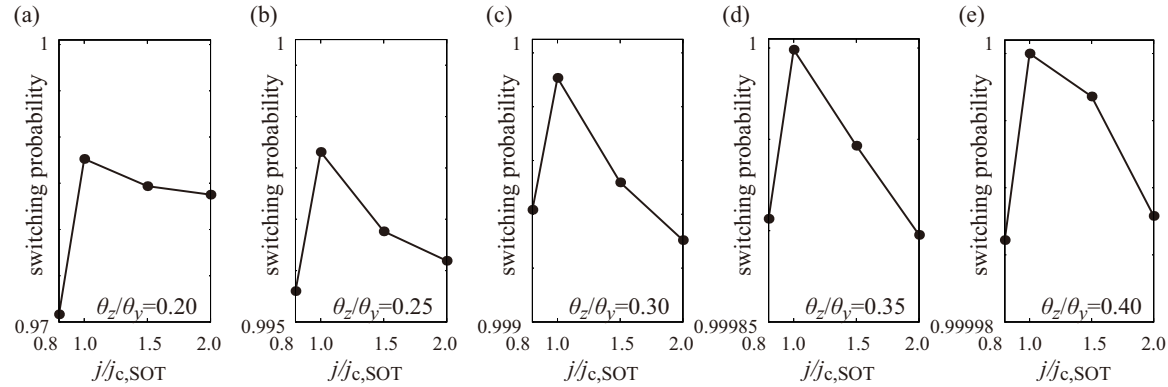

FIG. 4. Dependence of the magnetization switching probabilities on the electric current density, $j/j_{c,SOT}$ for ϑ_z/ϑ_y of (a) 0.20, (b) 0.25, (c) 0.30, (d) 0.35, and (e) 0.40.

These results partially explain the current dependence of the switching probability in Figs. 3 and 4, in particular for the large current cases ($j/j_{c,SOT} = 1.5$ and 2.0). As mentioned, a strong y-SOT originated from a large electric current density forces the magnetization to the in-plane (y) direction. When the magnetization locates close to the in-plane direction, even if $m_z < 0$, thermal fluctuation causes a probabilistic return to the initial state ($m_z = 1$). It results in the reduction of the switching probability, or equivalently, in an increase of the switching error. Accordingly, the switching probability decreases as the electric current density increases when $j/j_{c,SOT} \geqslant 1.0$. This is consistent with the result for $j/j_{c,SOT} = 1.0$, 1.5, and 2.0 shown in Figs. 3 and 4.

We should, however, recall that, for the case of small electric current density, the switching probability increases as the electric current density increases; see the switching probabilities for $j/j_{c,SOT} = 0.8$ and 1.0 in Figs. 3 and 4. This result indicates that the current dependence of the switching probability cannot be explained solely by the y-SOT. To clarify the switching mechanism in this small current region, an analysis on one temporal dynamics is not enough. Therefore, in the following sections, we perform statistical analysis and analytical calculation.

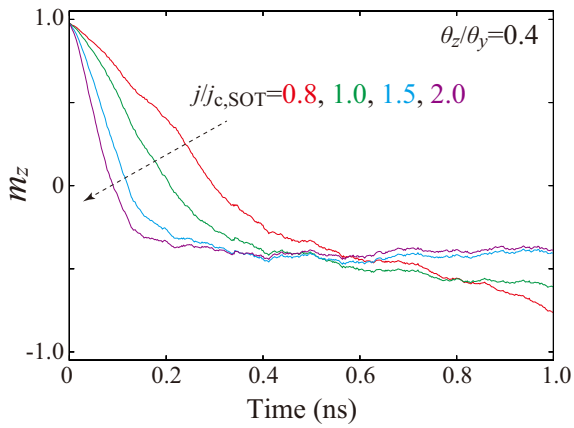

FIG. 5. Examples of temporal dynamics of magnetization (m_z) in the presence of electric current densities, $j/j_{SOT} = 0.8$ (red), 1.0 (green), 1.5 (blue), and 2.0 (purple). The value of $\vartheta_z/\vartheta_y = 0.4$.

B. Magnetization distribution

To clarify the dependence of the switching probability on the electric current density in small current region, we evaluate the distribution of m_z when the electric current density is turned off. Figure 6 shows the spectra of the distribution of m_z as a function of the tilt angle of the magnetization from the z axis, $\cos^{-1} m_z$, for various ϑ_z/ϑ_y. The initial and switched states correspond to 0° ($m_z = +1.0$) and 180° ($m_z = -1$) while the in-plane magnetized state corresponds to 90°. First, we notice that the peaks of the distribution move from close to the switched state to the in-plane magnetized state as the electric current density increases, which is consistent with m_z found in Fig. 5. Second, we notice that the distributions for large electric current densities ($j/j_{c,SOT} = 1.5$ and 2.0) are relatively sharp. This is because a strong y-SOT makes the magnetization dynamics approximately deterministic against thermal fluctuation. Third and importantly, the distribution for the small electric current density ($j/j_{c,SOT} = 0.8$) shows a large width, and m_z in some trials remains in the nonswitched ($m_z > 0$) state. The presence of such nonswitched trials results in reducing switching probability, even though the peak position of the distribution is closer to the switched state than those of the larger current densities.

The presence of the nonswitched state for the small electric current density ($j/j_{c,SOT} = 0.8$) is explained as follows. Recall that $j_{c,SOT}$ is the critical current density for the magnetization destabilization solely by the y-SOT. Therefore, y-SOT is insufficient to move the magnetization to the negative m_z region. Both y and z-SOTs are necessary for the magnetization switching. The z-SOT is necessary to move the magnetization to the region of $m_z < 0$. However, the switching by the z-SOT is similar to the conventional STT switching and thus, costs a long switching time because the STT switching accompanies the magnetization precession [16]. In particular, the time necessary to escape from the initial state dominates the switching time. The y-SOT contributes to reducing this time, even though its magnitude is smaller than the critical value, by moving the magnetization from the easy (z) axis immediately; see also Appendix, where we compare the magnetization dynamics in the presence of both torques and solely by the z-SOT. We should also recall that the switching speed is relatively slow for small current; see Appendix again. Accordingly, the magnetization sometimes remains near the initial

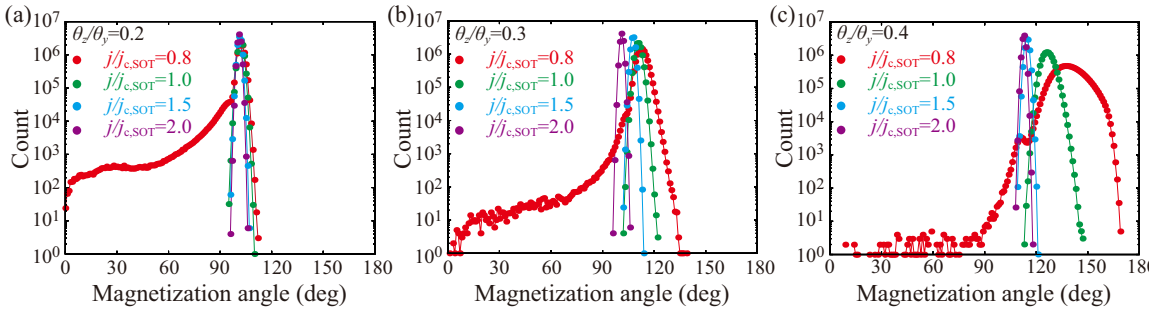

FIG. 6. Spectra of m_z when the electric current density is turned off, where j/j_{SOT} is 0.8 (red), 1.0 (green), 1.5 (blue), and 2.0 (purple), while ϑ_z/ϑ_y is (a) 0.2, (b) 0.3, and (c) 0.4. Note that the magnetization direction near $\theta = 0^\circ$ is the initial state, $\theta = 90^\circ$ is the in-plane magnetized state, and $\theta = 180^\circ$ is the switched state.

state for this case and leads to an increase of the switching error.

To summarize the analyses up to this point, the current dependence of the switching probability in Figs. 3 and 4 is explained from two viewpoints, as follows. In the small current region ($j/j_{c,SOT} \lesssim 1$), the switching probability increases as the electric current increases. This is because the number of the trials remained near the initial state decreases as the electric current density increases. In the large current region ($j/j_{c,SOT} \gtrsim 1$), in contrast, the y-SOT forces the magnetization to lie in the xy-plane and causes a probabilistic return after turning off the current. Therefore, the switching probability decreases as the electric current density increases. Accordingly, the switching probability is maximized when the electric current density is close to the critical value, $j_{c,SOT}$.

C. Steady state solution

The above analyses for the large current region are also verified by deriving a steady state solution of the LLG equation. By introducing the zenith and azimuth angles, θ and φ, as $\mathbf{m} = (\sin\theta\cos\varphi, \sin\theta\sin\varphi, \cos\theta)$, the steady state solutions of the LLG equation are determined by

$$p\sin\theta - \cos\theta\sin\varphi = 0, \tag{6}$$

$$\sin\theta\cos\theta - \frac{r}{2}\cos\varphi = 0. \tag{7}$$

For simplicity, we introduce dimensionless quantities r and p given by

$$r = \frac{j}{j_{c,SOT}}. \tag{8}$$

$$p = \frac{\vartheta_z}{\vartheta_y}. \tag{9}$$

A solution of $m_z = \cos\theta$ obtained from Eqs. (6) and (7) is given by

$$m_z = -\sqrt{\frac{4 - 3(1+p^2)r^2 + 2A^{1/3} + A^{2/3}}{6A^{1/3}}}, \tag{10}$$

where A is

$$A = 3[48p^2r^2 - 3(1 + 20p^2 - 8p^4)r^4 + 3(1+p^2)^3r^6]^{1/2} + 8 - 9(1-2p^2)r^2. \tag{11}$$

The steady state is determined as a result of the competition between two SOTs and the precessional torque due to the magnetic anisotropy field. The magnetic anisotropy field appears through the definition of $j_{c,SOT}$ in r, while two SOTs appear in p. The damping torque is proportional to $d\mathbf{m}/dt$ and thus, $j_{c,STT} \propto \alpha$ does not appear to determine the steady state ($d\mathbf{m}/dt = \mathbf{0}$) solution. In the low current region, z-SOT intends to move the magnetization near $m_z = -1$ while the y-SOT is compensated by the precessional torque and is insufficient to induce the switching [49]. Thus, the steady state is mainly determined by the z-SOT and locates near $m_z = -1$. When the electric current density exceeds $j_{c,SOT}$, the y-SOT overcomes the precessional torque. Then, the contribution of the y-SOT to determine the steady state becomes relatively large. Since the y-SOT prefers to fix the magnetization to the y-direction, the steady state moves toward $m_z = 0$. In the large current limit ($r \to \infty$), the steady state solution is determined by the competition between two SOTs, and Eq. (10) saturates to $-1/\sqrt{1+(1/p^2)}$. This value becomes 0 (-1) in the limit of $p \to 0$ (∞), in which only the y (z)-SOT acts on the magnetization and moves it to the in-plane (switched) direction.

Figure 7(a) shows the dependence of Eq. (10) on $j/j_{c,SOT}$ for $\vartheta_z/\vartheta_y = 0.4$. The result is partially consistent with the temporal dynamics shown in Fig. 5. For example, m_z deviates from the switched state ($m_z = -1.0$) as the electric current density increases. The steady state solution shows a sudden change near $j/j_{c,SOT} = 1.0$. The values of m_z for $j/j_{c,SOT} = 1.5$ and 2.0 in Fig. 7 are close to those in Fig. 5. Therefore, we can conclude that the magnetization for $j/j_{c,SOT} = 1.5$ and 2.0 in Fig. 5 reaches the steady state (the value of m_z saturates to -0.37 when $j \to \infty$ in this case). We should, however, notice that the values of m_z between the temporal dynamics in Fig. 5 and the steady state solution in Fig. 7 are different when the electric current density is small ($j/j_{c,SOT} = 0.8$ and 1.0). This is because the y-SOT in Fig. 5 is small and the switching speed is slow; therefore, m_z in Fig. 5 does not reach the steady state before turning off the electric current density. This point is verified by evaluating the values of m_z at the pulse width ($t = 1.0$ ns) and the magnetization reaches the steady state ($t \to \infty$) from the numerical simulation of the LLG equation at zero temperature; see Figs. 7(b) and 7(c), which show m_z at $t = 1.0$ and 20.0 ns. Note that Figs. 7(b) and 7(c) are obtained by the numerical simulation with the constant electric current density, i.e., j is kept constant for

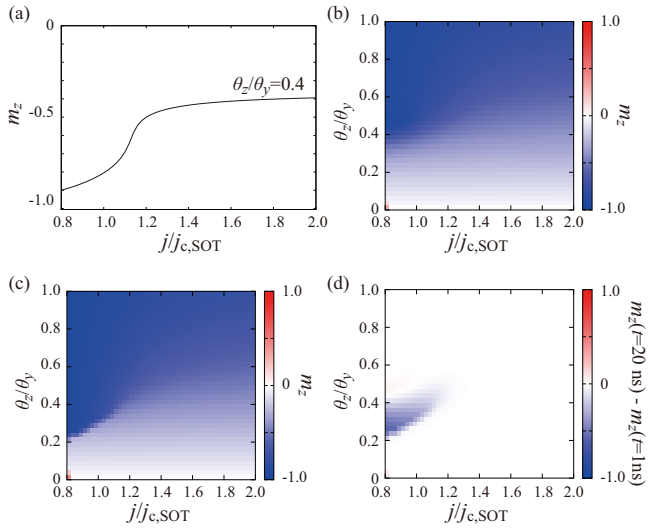

FIG. 7. (a) Dependence of the steady state solution of m_z, given by Eq. (10), on the electric current density with respect to the critical value, $j/j_{c,SOT}$. The value of ϑ_z/ϑ_y is 0.4. Dependence of m_z at (b) $t = 1.0$ ns and (c) $t = 20.0$ ns estimated by solving the LLG equation at zero temperature on $j/j_{c,SOT}$ and ϑ_z/ϑ_y is also shown. Electric current density is kept constant for 20.0 ns here, while in other simulations only the 1.0 ns current pulse was used. The differences between magnetic moment projections m_z calculated for $t = 20.0$ ns and $t = 1.0$ ns are shown in the panel (d).

$t = 20.0$ ns, while the electric current is turned off at $t = 1.0$ ns in other simulations such as Fig. 1(b). This was necessary for understanding whether the 1.0 ns current pulse is sufficient for bringing magnetization to the switched state (see also Appendix, where it is confirmed from the temporal dynamics that $t = 20.0$ ns is enough to estimate the saturated value of m_z). We confirm that the values of m_z between Figs. 7(b) and 7(c) are the same for large current region ($j/j_{c,SOT} \gtrsim 1.0$) while they are different for the small current region ($j/j_{c,SOT} \lesssim 1.0$); see also Fig. 7(d), which shows their difference, $m_z(t = 20\ \text{ns}) - m_z(t = 1\ \text{ns})$. It indicates that the magnetization reaches (does not reach) the steady state when the current is turned off for the large (small) current region. In Fig. 7, the lowest current is limited to $j/j_{c,SOT} = 0.8$ because we are interested in a steady state satisfying $m_z < 0$ here. The phase diagram for a wider range of currents is provided in Appendix.

These results explain the current dependence of the switching probability in the large current region ($j/j_{c,SOT} \gtrsim 1$) again. When the electric current density is large, m_z reaches the steady state during the application of the current pulse. The magnetization moves from close to the switched state to the in-plane magnetized state as the electric current density increases due to the large y-SOT. It is consistent with the result in Fig. 6, where the peak of the spectra moves to the in-plane direction (90°) when $j/j_{c,SOT}$ changes from 1.5 to 2.0. As a result, the rate of the probabilistic return to the initial state increases. Therefore, the switching probability decreases as the electric current density increases. On the other hand, the steady state solution in Fig. 7 cannot be compared to the temporal dynamics in Fig. 5 directly when the current density is relatively small ($j/j_{c,SOT} \lesssim 1$). The existence of such a difference, however, still signifies that the switching behavior must be separated into two regions, $j/j_{c,SOT} \gtrsim 1$ and $j/j_{c,SOT} \lesssim 1$, in order to understand the current dependence of the switching probability.

At the end of this subsection, we provide comments for readers who are interested in the steady state solution from the mathematical viewpoint. Note that Eq. (10) is not a unique solution of the LLG equation in a steady state. There are other steady state solutions of the LLG equation, and the magnetization reaches one of these possible states, depending on the values of the parameters and the initial condition. For example, $m_z = \pm 1$ are the steady state solutions in the absence of SOTs ($j \to 0$). Equation (10) represents one of the steady state solutions near the switched state. Therefore, it may differ from to the solution of numerical simulation in some cases; for example, while Fig. 7(a) shows that $m_z \to -1$ in the limit of $j \to 0$, the solution of numerically solved LLG equation does not reach this switched state because of the absence of SOTs. In the present work, however, since the current density is always finite, Eq. (10) works for the most cases. Note also that Eq. (10) is applicable to some values of r and p, however, it becomes a complex number and provides unphysical solution for the other values of r and p. Some of the other steady state solutions are tedious and also give unphysical solutions, depending on the values of r and p. For Eq. (10), for example, the quantity A in Eq. (11) is a real number for an arbitrary r only when $p > 1/(2\sqrt{2}) \simeq 0.35$; however, when $p < 1/(2\sqrt{2})$, the discriminant of the square root in Eq. (11) becomes negative, and thus, A becomes a complex number for some values of r (especially near $r \simeq 1$). Therefore, we show Eq. (10) only for $p = \vartheta_z/\vartheta_y = 0.40$ in Fig. 7(a). We, however, notice that, in reality, Eq. (10) is still a real number and well describes the steady state solution even for a small $p[< 1/(2\sqrt{2})]$ for a wide range of r. In addition, without such a strict mathematical treatment of the steady state solution, the origin of the switching error can be well analyzed by Eq. (10), as done above. Therefore, we believe that Eq. (10) is enough for the present work.

D. Applicability of present analysis

One might consider that the decrease of the switching probability as the electric current density increases in the large current region also appears for the conventional SOT switching, where only the y-SOT exists and an in-plane external magnetic field is applied to devices. Although a similar role of the y-SOT may exist in the conventional SOT switching, it is difficult to compare the present work to it due to the following reason. An issue in the conventional SOT switching is a sensitivity of the switching condition on the electric current density even at zero temperature [47]. The meaning of the sensitivity is as follows. For certain current magnitude larger than a critical value, the magnetization moves close to the switched state by the SOT, and relaxes to the switched state when the current is turned off. When the current magnitude is slightly changed, however, the magnetization returns to the initial state after turning off the current. This is in contrast to the conventional STT switching, where the magnetization switching always occurs when the current magnitude exceeds the critical

value [16]. This sensitivity in the conventional SOT switching originates from precessional dynamics of the magnetization around the external magnetic field after turning off the current and has a deterministic nature, not a probabilistic one due the thermal fluctuation. Such precessional dynamics, and thus the sensitivity of the switching condition on the current, are unavoidable as the electric current density increases [49]. The existence of this sensitivity provides an additional difficulty to analyze the switching probability by the conventional SOT switching. Although the previous work observed a monotonic increase of the switching probability as the electric current density increases, its current value is limited to a relatively low current region [17]; thus, it remains unclear how these factors (the probabilistic return due to thermal fluctuation and the precessional dynamics around the external magnetic field) affect the switching probability in a large current region. We keep this issue as a future work.

Let us also comment on the role of the pulse width on the switching probability. Regarding the above results, one might consider that the result depends on the pulse width of the electric current. When the pulse width is sufficiently long, high switching probability will be achieved even if the electric current density is small (when the condition $j/j_{c,\mathrm{STT}} > 1$ is satisfied). Such a switching, however, is basically similar to the conventional STT switching and has been already studied extensively [16]. Therefore, such a switching is out of interest in this work. When the pulse width is sufficiently short, on the other hand, large current is necessary to make the switching time short. Therefore, the switching probability increases as the electric current density increases. In such a case, a careful evaluation of the pulse shape from a circuit simulator might be necessary, as in the case of a different switching scheme [56], which is beyond the scope of this work. In our opinion, the value of the pulse width used in this work (1.0 ns, or more generally on the order of a few nanoseconds) is reasonable for developing SOT-based spintronics applications. Therefore, we believe that the present results will be applicable to a wide range of spintronics research even in the presence of such an applicable range.

IV. CONCLUSION

In conclusion, the magnetization switching probability due to SOTs caused by spin currents generated in a ferromagnetic electrode was studied theoretically. The numerical simulation of the LLG equation indicates that the probability of the magnetization switching is maximized when the electric current density is close to the critical value for the magnetization destabilization solely by the y-SOT. This is contrary to the intuition, as well as the previous reports, that the switching probability increases as the electric current density increases. The origin of the increase of the switching error was investigated by analyzing the temporal dynamics, evaluating the spectra of the magnetization distribution, and deriving an analytical solution of the steady state LLG equation. These analyses reveal that the maximization of the switching probability is a result of the current dependence of the switching probability in two different current regions. In the low current region, the time necessary to escape from the initial state becomes relatively long. Then, the magnetization in some trials remains near the initial state when the current is turned off and results in a switching error. Therefore, a large current is necessary to increase the switching speed. As a result, the switching probability increases as the electric current density increases. When the electric current density exceeds the critical value, on the other hand, the magnetization immediately saturates to the steady state due to a strong y-SOT. Since the y-SOT moves the magnetization to the in-plane direction, the magnetization in a steady state changes from close to the switched state to the in-plane magnetized state. The change of the steady state causes a probabilistic return of the magnetization due to thermal fluctuation and results in an increase of the switching error. Therefore, the switching probability decreases as the electric current density increases. In summary, the switching probability is maximized when the electric current density is close to the critical value, and an application of large electric current does not guarantee a high switching probability.

ACKNOWLEDGMENTS

This work was supported by funding from the TDK Corporation.

T.T. performed numerical simulation and developed theoretical analyses. T.T. and M.H. conceptualized the work and wrote the paper with review by S.I., S.O., K.N., T.S., and S.M.

DATA AVAILABILITY

The data that support the findings of this article are not publicly available. The data are available from the authors upon reasonable request.

APPENDIX: ZERO TEMPERATURE DYNAMICS TO STEADY STATE

In Sec. III A, we described that the magnetization for $j/j_{c,\mathrm{SOT}} = 0.8$ and 1.0 does not reach a steady state, while the magnetization for $j/j_{c,\mathrm{SOT}} = 1.5$ and 2.0 saturates its direction. This argument was confirmed in Sec. III C by deriving an analytical solution of the steady state. Here, we confirm the argument again from the temporal solution of the LLG equation.

In Figs. 8(a)–8(d), we show the temporal dynamics of m_z for $j/j_{c,\mathrm{SOT}}$ of 0.8, 1.0, 1.5, and 2.0, respectively, by black lines. Here, the temperature is set to be zero, and the electric current density is constant to estimate the steady state. These results confirm that the magnetization for $j/j_{c,\mathrm{SOT}} = 0.8$ and 1.0 is not saturated to the steady state solution when $t =$ 1.0 ns, while the magnetization for $j/j_{c,\mathrm{SOT}} = 1.5$ and 2.0 immediately reaches the steady state during the application of the electric current density.

In Sec. III B, we described that the switching speed by the z-SOT becomes fast as the electric current density increases. This argument can be verified both numerically and analytically. First, we show the temporal dynamics of m_z solely by the z-SOT (or in other words, we neglect the y-SOT) in Fig. 8 by blue lines. Since $\vartheta_y = 0.3$ and $\vartheta_z/\vartheta_y = 0.4$ were mainly used in the main text, we use $\vartheta_z = 0.12$ in $H_{\mathrm{SOT},z}$ in the following. On the other hand, we set $H_{\mathrm{SOT},y} = 0$ because we are interested in the magnetization dynamics solely by the

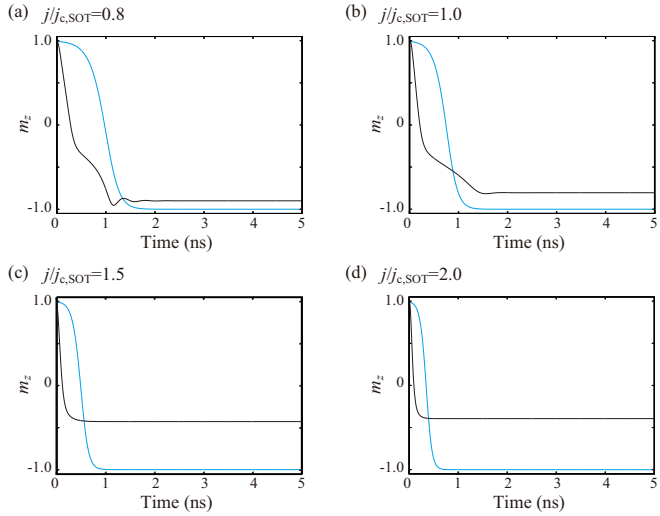

FIG. 8. Temporal dynamics of m_z at zero temperature for $j/j_{c,SOT}$ of (a) 0.8, (b) 1.0, (c) 1.5, and (d) 2.0. A constant electric current is assumed in this calculation. Black and blue lines correspond to the dynamics for $H_{SOT,y} \neq 0$ and $H_{SOT,y} = 0$, respectively.

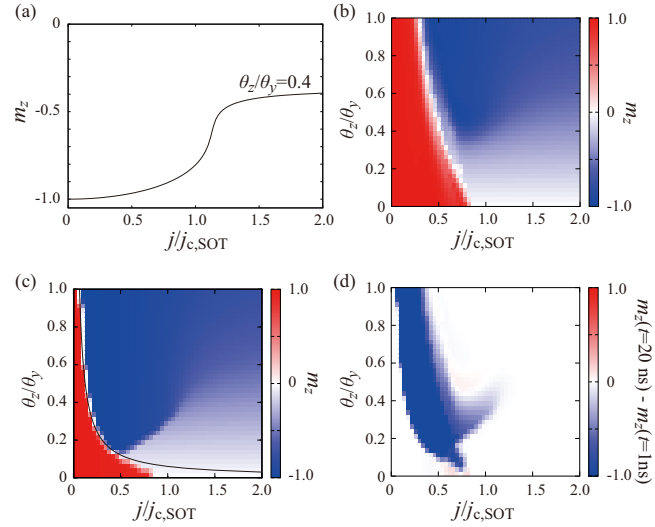

FIG. 9. Extensions of Fig. 7 to lower current region. A black solid line in (c) is derived from Eq. (4).

z-SOT. Note that the initial state of the magnetization is set to be $\mathbf{m}(0) = (\sin\theta_0, 0, \cos\theta_0)$ with $\theta_0 = 1/\sqrt{\Delta_0}$ [50], in contrast to $\mathbf{m}(0) = +\mathbf{e}_z$ before thermalization in the main text. This is because a finite tilt angle of the magnetization is necessary to make the z-SOT finite at the initial state. Figures 8(a)–8(d) indicate that the switching speed becomes faster as the electric current density increases. This result can also be confirmed by deriving an analytical solution of the LLG equation as

$$\alpha\gamma H_K t = -\frac{s}{s^2-1}(\tanh^{-1}\cos\theta - \tanh^{-1}\cos\theta_0) + \frac{1}{2(s^2-1)}\ln\frac{1-\cos^2\theta}{1-\cos^2\theta_0} - \frac{1}{s^2-1}\ln\frac{s-\cos\theta}{s-\cos\theta_0}, \tag{A1}$$

where $s = j/j_{c,STT}$. Equation (A1) provides the magnetization tilt angle $\theta = \cos^{-1} m_z$ at time t. We note that this equation is applicable for an arbitrary value of s. When the z-SOT is larger than the damping torque and thus, $s > 1$, the magnetization moves from the initial state θ_0 to the switched direction, $\theta = \pi$, i.e., $\theta(t) > \theta_0$. On the other hand, when the z-SOT is smaller than the damping torque ($s < 1$), the magnetization relaxes from θ_0 to $\theta = 0$, i.e., $\theta(t) < \theta_0$. Therefore, the time t becomes positive value by substituting $\theta > (<)\theta_0$ into Eq. (A1) when $s > (<)1$. If we substitute the opposite value, i.e., $\theta < (>)\theta_0$ for $s > (<)1$ into Eq. (A1), t becomes negative because it describes a process going backward to the past. In both cases, t is the real value. In the present study, $j_{c,STT} = 13$ MA/cm^2 by using the parameters in the mentioned above, while $j_{c,SOT} = 89$ MA/cm^2, as already mentioned in the main text [note that $j_{c,SOT}$ does not appear in Eq. (A1) because only the z-SOT is taken into account here, although we use the value of $j_{c,SOT}$ to give the value of j quantitatively]. Accordingly, $j/j_{c,STT} > 1$ is satisfied in all cases in Fig. 8; therefore, θ increases as time increases, and the magnetization switching is achieved. Equation (A1) indicates that the switching speed by the z-SOT becomes shorter as the electric current density increases. Equation (A1) also implies that the time necessary to tilt from the z axis becomes longer when the initial state (θ_0) is close to the z axis. Therefore, we concluded that both the y and z-SOTs prompt the switching in the low current region. The y-SOT contributes to moving the magnetization from the z axis and reduces the switching time, even though the current density is below the critical value and thus, the y-SOT cannot induce the switching solely by itself. The z-SOT contributes to moving the magnetization close to the switched state.

In Figs. 7(a)–7(d) in Sec. III C, we showed the analytical solution of the steady state, the values of m_z at $t = 1.0$ ns and 20.0 ns and their difference obtained from the numerical simulation, respectively. The lowest electric current density is limited to $j/j_c = 0.8$ because we are interested in the magnetization switching, and thus, m_z should become at least negative for given parameters. One might be, however, interested in extending the results for the lower current region. Figure 9 summarizes the extension of Fig. 7 to $j/j_c = 0$. Recall that the magnetization does not move to the region of negative m_z when the current is small, while Eq. (10) is derived by assuming $m_z < 0$; therefore, there are differences between the analytical solution in Fig. 9(a) [or Eq. (10)] and the numerical solution in Fig. 9(c) for the steady state. Comparing Figs. 9(b)–9(d), we notice that the region of $m_z \simeq 1.0$ in Fig. 9(b) is greatly suppressed in Fig. 9(c), i.e., the magnetization does not reach the steady state within 1.0 ns (recall that the electric current is kept being constant in these calculations, and thus, the magnetization can move to the switched direction by the SOTs even after $t = 1.0$ ns). We notice that the boundary between $m_z > 0$ and $m_z < 0$ in the low current region of Fig. 9(c) is well fitted by Eq. (4), which is shown by a black solid line in the figure. This result supports the above argument that the z-SOT moves the magnetization close to the switched state when the electric current density is small.

[1] L. Liu, C.-F. Pai, Y. Li, H. W. Tseng, D. C. Ralph, and R. A. Buhrman, Spin-torque switching with the giant spin Hall effect of tantalum, Science **336**, 555 (2012).

[2] L. Liu, O. J. Lee, T. J. Gudmundsen, D. C. Ralph, and R. A. Buhrman, Current-induced switching of perpendicularly magnetized magnetic layers using spin torque from the spin Hall effect, Phys. Rev. Lett. **109**, 096602 (2012).

[3] C.-F. Pai, L. Liu, Y. Li, H. W. Tseng, D. C. Ralph, and R. A. Buhrman, Spin transfer torque devices utilizing the giant spin Hall effect of tungsten, Appl. Phys. Lett. **101**, 122404 (2012).

[4] M. I. Dyakonov and V. I. Perel, Current-induced spin orientation of electrons in semiconductors, Phys. Lett. A **35**, 459 (1971).

[5] J. E. Hirsch, Spin Hall effect, Phys. Rev. Lett. **83**, 1834 (1999).

[6] S. Zhang, Spin Hall effect in the presence of spin diffusion, Phys. Rev. Lett. **85**, 393 (2000).

[7] J. C. Slonczewski, Current-driven excitation of magnetic multilayers, J. Magn. Magn. Mater. **159**, L1 (1996).

[8] L. Berger, Emission of spin waves by a magnetic multilayer traversed by a current, Phys. Rev. B **54**, 9353 (1996).

[9] J. A. Katine, F. J. Albert, R. A. Buhrman, E. B. Myers, and D. C. Ralph, Current-driven magnetization reversal and spin-wave excitations in Co/Cu/Co pillars, Phys. Rev. Lett. **84**, 3149 (2000).

[10] E. B. Myers, F. J. Albert, J. C. Sankey, E. Bonet, R. A. Buhrman, and D. C. Ralph, Thermally activated magnetic reversal induced by a spin-polarized current, Phys. Rev. Lett. **89**, 196801 (2002).

[11] S. I. Kiselev, J. C. Sankey, I. N. Krivorotov, N. C. Emley, R. J. Schoelkopf, R. A. Buhrman, and D. C. Ralph, Microwave oscillations of a nanomagnet driven by a spin-polarized current, Nature (London) **425**, 380 (2003).

[12] H. Kubota, A. Fukushima, Y. Ootani, S. Yuasa, K. Ando, H. Maehara, K. Tsunekawa, D. D. Djayaprawira, N. Watanabe, and Y. Suzuki, Evaluation of spin-transfer switching in CoFeB/MgO/CoFeB magnetic tunnel junctions, Jpn. J. Appl. Phys. **44**, L1237 (2005).

[13] I. N. Krivorotov, N. C. Emley, J. C. Sankey, S. I. Kiselev, D. C. Ralph, and R. A. Buhrman, Time-domain measurements of nanomagnet dynamics driven by spin-transfer torques, Science **307**, 228 (2005).

[14] Z. Diao, D. Apalkov, M. Pakala, Y. Ding, A. Panchula, and Y. Huai, Spin transfer switching and spin polarization in magnetic tunnel junctions with MgO and AlO_x barriers, Appl. Phys. Lett. **87**, 232502 (2005).

[15] B. Dieny and I. L. Prejbeanu, in *Introduction to Magnetic Random-Access Memory*, edited by B. Dieny, R. B. Goldfarb, and K.-J. Lee (Wiley-IEEE Press, Hoboken, 2016), Chap. 5.

[16] J. Z. Sun, Spin-current interaction with a monodomain magnetic body: A model study, Phys. Rev. B **62**, 570 (2000).

[17] K.-S. Lee, S.-W. Lee, B.-C. Min, and K.-J. Lee, Thermally activated switching of perpendicular magnet by spin-orbit spin torque, Appl. Phys. Lett. **104**, 072413 (2014).

[18] G. Yu, P. Upadhyaya, Y. Fan, J. G. Alzate, W. Jiang, K. L. Wong, S. Takei, S. A. Bender, L.-T. Chang, Y. Jiang, M. Lang, J. Tang, Y. Wang, Y. Tserkovnyak, P. K. Amiri, and K. L. Wang, Switching of a perpendicular magnetization by spin-orbit torques in the absence of external magnetic fields, Nat. Nanotechnol. **9**, 548 (2014).

[19] L. You, O. Lee, D. Bhowmik, D. Labanowski, J. Hong, J. Bokor, and S. Salahuddin, Switching of perpendicularly polarized nanomagnets with spin orbit torque without an external magnetic field by engineering a tilted anisotropy, Proc. Natl. Acad. Sci. USA **112**, 10310 (2015).

[20] J. Torrejon, F. Garcia-Sanchez, T. Taniguchi, J. Sinha, S. Mitani, J.-V. Kim, and M. Hayashi, Current-driven asymmetric magnetization switching in perpendicularly magnetized CoFeB/MgO heterostructures, Phys. Rev. B **91**, 214434 (2015).

[21] S. Fukami, T. Anekawa, C. Zhang, and H. Ohno, Magnetization switching by spin-orbit torque in an antiferromagnet-ferromagnet bilayer system, Nat. Mater. **15**, 535 (2016).

[22] Y.-C. Lau, D. Betto, K. Rode, J. M. D. Coey, and P. Stamenov, Spin-orbit torque switching without an external field using interlayer exchange coupling, Nat. Nanotechnol. **11**, 758 (2016).

[23] M. Wang, W. Cai, D. Zhu, Z. Wang, J. Kan, Z. Zhao, K. Cao, Z. Wang, Y. Zhang, T. Zhang, C. Park, J.-P. Wang, A. Fert, and W. Zhao, Field-free switching of a perpendicular magnetic tunnel junction through the interplay of spin-orbit and spin-transfer torques, Nat. Electron. **1**, 582 (2018).

[24] E. Grimaldi, V. Krizakova, G. Sala, F. Yasin, S. Couet, G. S. Kar, K. Garello, and P. Gambardella, Single-shot dynamics of spin-orbit torque and spin transfer torque switching in three-terminal magnetic tunnel junctions, Nat. Nanotechnol. **15**, 111 (2020).

[25] S. Pathak, C. Youm, and J. Hong, Impact of spin-orbit torque on spin-transfer torque switching in magnetic tunnel junctions, Sci. Rep. **10**, 2799 (2020).

[26] C. Zhang, Y. Takeuchi, S. Fukami, and H. Ohno, Field-free and sub-ns magnetization switching of magnetic tunnel junctions by combining spin-transfer torque and spin-orbit torque, Appl. Phys. Lett. **118**, 092406 (2021).

[27] D. H. Kang and M. Shin, Critical switching current density of magnetic tunnel junction with shape perpendicular magnetic anisotropy through the combination of spin-transfer and spin-orbit torques, Sci. Rep. **11**, 22842 (2021).

[28] T. Taniguchi, J. Grollier, and M. D. Stiles, Spin-transfer torques generated by the anomalous Hall effect and anisotropic magnetoresistance, Phys. Rev. Appl. **3**, 044001 (2015).

[29] V. P. Amin and M. D. Stiles, Spin transport at interfaces with spin-orbit coupling: Formalism, Phys. Rev. B **94**, 104419 (2016).

[30] V. P. Amin and M. D. Stiles, Spin transport at interfaces with spin-orbit coupling: Phenomenology, Phys. Rev. B **94**, 104420 (2016).

[31] V. P. Amin, J. Zemen, and M. D. Stiles, Interface-generated spin currents, Phys. Rev. Lett. **121**, 136805 (2018).

[32] V. P. Amin, J. Li, M. D. Stiles, and P. M. Haney, Intrinsic spin currents in ferromagnets, Phys. Rev. B **99**, 220405(R) (2019).

[33] A. Davidson, V. P. Amin, W. S. Aljuaid, P. M. Haney, and X. Fan, Perspectives of electrically generated spin currents in ferromagnetic materials, Phys. Lett. A **384**, 126228 (2020).

[34] G. Qu, K. Nakamura, and M. Hayashi, Magnetization direction dependent spin Hall effect in 3*d* ferromagnets, Phys. Rev. B **102**, 144440 (2020).

[35] G. G. Baez Flores, A. A. Kovalev, M. van Schilfgaarde, and K. D. Belashchenko, Generalized magnetoelectronic circuit theory and spin relaxation at interfaces in magnetic multilayers, Phys. Rev. B **101**, 224405 (2020).

[36] K.-W. Kim and K.-J. Lee, Generalized spin drift-diffusion formalism in the presence of spin-orbit interaction of ferromagnets, Phys. Rev. Lett. **125**, 207205 (2020).

[37] Y. Miura and K. Masuda, First-principles calculations on the spin anomalous Hall effect of ferromagnetic alloys, Phys. Rev. Mater. **5**, L101402 (2021).

[38] S. Iihama, T. Taniguchi, K. Yakushiji, A. Fukushima, Y. Shiota, S.Tsunegi, R. Hiramatsu, S. Yuasa, Y. Suzuki, and H. Kubota, Spin-transfer torque induced by the spin anomalous Hall effect, Nat. Electron. **1**, 120 (2018).

[39] S.-H. C. Baek, V. P. Amin, Y.-W. Oh, G. Go, S.-J. Lee, G.-H. Lee, K.-J. Kim, M. D. Stiles, B.-G. Park, and K.-J. Lee, Spin currents and spin-orbit torques in ferromagnetic trilayers, Nat. Mater. **17**, 509 (2018).

[40] Y.-W. Oh, J. Ryu, J. Kang, and B.-G. Park, Material and thickness investigation in ferromagnet/Ta/CoFeB trilayers for enhancement of spin-orbit torque and field-free switching, Adv. Electron. Mater. **5**, 1900598 (2019).

[41] T. Seki, S. Iihama, T. Taniguchi, and K. Takanashi, Large spin anomalous Hall effect in $L1_0$–FePt: Symmetry and magnetization switching, Phys. Rev. B **100**, 144427 (2019).

[42] Y. Hibino, K. Hasegawa, T. Koyama, and D. Chiba, Spin-orbit torque generated by spin-orbit precession effect in Py/Pt/Co trilayer structure, APL Mater. **8**, 041110 (2020).

[43] Y. Koike, S. Iihama, and S. Mizukami, Composition dependence of the spin-anomalous Hall effect in a ferromagnetic Fe–Co alloy, Jpn. J. Appl. Phys. **59**, 090907 (2020).

[44] Y. Hibino, T. Taniguchi, K. Yakushiji, A. Fukushima, H. Kubota, and S. Yuasa, Giant charge-to-spin conversion in ferromagnet via spin-orbit coupling, Nat. Commun. **12**, 6254 (2021).

[45] G. Choi, J. Ryu, S. Lee, J. Kang, N. Noh, J. M. Yuk, and B.-G. Park, Thickness dependence of interface-generated spin currents in ferromagnet/Ti/CoFeB trilayers, Adv. Mater. Interface **9**, 2201317 (2022).

[46] T. Taniguchi, S. Isogami, S. Okame, K. Nakada, E. Komura, T. Sasaki, S. Mitani, and M. Hayashi, Probability of spin-orbit torque driven magnetization switching assisted by spin-transfer torque, Phys. Rev. B **108**, 134431 (2023).

[47] K.-S. Lee, S.-W. Lee, B.-C. Min, and K.-J. Lee, Theoretical current for switching of a perpendicular magnetic layer induced by spin Hall effect, Appl. Phys. Lett. **102**, 112410 (2013).

[48] H. Morise and S. Nakamura, Relaxing-precessional magnetization switching, J. Magn. Magn. Mater. **306**, 260 (2006).

[49] T. Taniguchi, Theoretical condition for switching the magnetization in a perpendicularly magnetized ferromagnet via the spin Hall effect, Phys. Rev. B **100**, 174419 (2019).

[50] T. Taniguchi, K. Yamada, and Y. Nakatani, Critical current formula of perpendicularly magnetized magnetic random access memory revisited, Jpn. J. Appl. Phys. **58**, 058001 (2019).

[51] M. Oogane, T. Wakitani, S. Yakata, R. Yilgin, Y. Ando, A. Sakuma, and T. Miyazaki, Magnetic damping in ferromagnetic thin films, Jpn. J. Appl. Phys. **45**, 3889 (2006).

[52] W. F. Brown Jr., Thermal fluctuations of a single-domain particle, Phys. Rev. **130**, 1677 (1963).

[53] T. Taniguchi, S. Isogami, Y. Shiokawa, Y. Ishitani, E. Komura, T. Sasaki, S. Mitani, and M. Hayashi, Magnetization switching probability in the dynamical switching regime driven by spin-transfer torque, Phys. Rev. B **106**, 104431 (2022).

[54] A. V. Khvalkovskiy, D. Apalkov, S. Watts, R. Chepulskii, R. S. Beach, A. Ong, X. Tang, A. Driskill-Smith, W. H. Butler, P. B. Visscher, D. Lottis, E. Chen, V. Nikitin, and M. Krounbi, Basic principles of STT-MRAM cell operation in memory arrays, J. Phys. D: Appl. Phys. **46**, 074001 (2013).

[55] D. Apalkov, B. Dieny, and J. M. Slaughter, Magnetoresistive random access memory, Proc. IEEE **104**, 1796 (2016).

[56] H. Lee, A. Lee, S. Wang, F. Ebrahimi, P. Gupta, P. K. Amiri, and K. L. Wang, A word line pulse circuit technique for reliable magnetoelectric random access memory, IEEE Trans. Very Large Scle Integr. (VLSI) Syst. **25**, 2027 (2017).